Hot-Spot Mix in Ignition-Scale Inertial Confinement Fusion Targets

S. P. Regan,[1] R. Epstein,[1] B. A. Hammel,[2] L. J. Suter,[2] H. A. Scott,[2] M. A. Barrios,[2] D. K. Bradley,[2] D. A. Callahan,[2] C. Cerjan,[2] G. W. Collins,[2] S. N. Dixit,[2] T. Döppner,[2] M. J. Edwards,[2] D. R. Farley,[2] K. B. Fournier,[2] S. Glenn,[2] S. H. Glenzer,[2] I. E. Golovkin,[3] S. W. Haan,[2] A. Hamza,[2] D. G. Hicks,[2] N. Izumi,[2] O. S. Jones,[2] J. D. Kilkenny,[2,6] J. L. Kline,[4] G. A. Kyrala,[4] O. L. Landen,[2] T. Ma,[2] J. J. MacFarlane,[3] A. J. MacKinnon,[2] R. C. Mancini,[5] R. L. McCrory,[1,*] N. B. Meezan,[2] D. D. Meyerhofer,[1,*] A. Nikroo,[6] H.-S. Park,[2] J. Ralph,[2] B. A. Remington,[2] T. C. Sangster,[1] V. A. Smalyuk,[2] P. T. Springer,[2] and R. P. J. Town[2]

[1]*Laboratory for Laser Energetics, University of Rochester, Rochester, New York 14623, USA*
[2]*Lawrence Livermore National Laboratory, Livermore, California 94551, USA*
[3]*Prism Computational Sciences, Madison, Wisconsin 53711, USA*
[4]*Los Alamos National Laboratory, Los Alamos, New Mexico 87545, USA*
[5]*University of Nevada, Reno, Nevada 89557, USA*
[6]*General Atomics, San Diego, California 92186, USA*

(Received 23 November 2011; revised manuscript received 4 April 2013; published 22 July 2013)

Mixing of plastic ablator material, doped with Cu and Ge dopants, deep into the hot spot of ignition-scale inertial confinement fusion implosions by hydrodynamic instabilities is diagnosed with x-ray spectroscopy on the National Ignition Facility. The amount of hot-spot mix mass is determined from the absolute brightness of the emergent Cu and Ge K-shell emission. The Cu and Ge dopants placed at different radial locations in the plastic ablator show the ablation-front hydrodynamic instability is primarily responsible for hot-spot mix. Low neutron yields and hot-spot mix mass between 34(−13, +50) ng and 4000(−2970, +17 160) ng are observed.

DOI: 10.1103/PhysRevLett.111.045001 PACS numbers: 52.57.−z, 52.38.Kd, 52.38.Ph, 52.70.La

Inertial confinement fusion (ICF) depends on the formation of a central hot spot with sufficient temperature and areal density for ignition (i.e., when the fusion energy exceeds the laser energy incident on the target) [1,2]. Laser-driven hohlraums are used to accelerate targets via x-ray ablation [1,2] at the 192-beam, 351-nm, 1.8-MJ National Ignition Facility (NIF) [3]. Shock-timing [4,5], implosion-velocity [6], and symmetry [7,8] experiments on the NIF are underway with ignition-scale targets [5,9] to optimize the hot-spot formation. The concentric spherical layers of current NIF ignition targets consist of a plastic Ge-doped or Si-doped ablator surrounding a thin shell of cryogenic thermonuclear fuel (i.e., hydrogen isotopes), with fuel vapor filling the interior volume [10]. Deuterium–tritium (DT) fuel is directed inside the ablator shell using a fill tube, and a DT-ice layer is formed using the beta-layering technique [11]. As the target implodes, the fuel vapor is compressed and forms a hot spot as the fuel layer decelerates. The hot spot contains $\sim 2 \times 10^4$ ng of DT mass, which undergoes fusion reactions. ICF relies on the DT-fusion alpha particles depositing their energy in the hot spot, causing the hot-spot temperature to rise sharply and a thermonuclear burn wave to propagate out through the surrounding cold and dense DT fuel. Ignition is predicted to occur when the temperature and areal density of the hot spot reach a minimum of 5 keV and 0.3 g/cm^2, respectively [10]. To date, experiments on the NIF have not achieved ignition.

Radiative and conductive losses from the hot spot will be increased by hydrodynamic instabilities [10,12]. Bright spots observed in broadband, gated x-ray implosion images for photon energies greater than 8 keV provide an indication that hot-spot mix may be occurring in NIF implosions [13]. Enhanced x-ray production relative to neutron yield is also being investigated as a mix diagnostic [14]. However, these methods are silent on what part of the shell the mix mass material comes from. The tracer-layer technique described herein provides insight for the physical mechanism that caused the ablator to mix into the hot spot. The Richtmyer–Meshkov and Rayleigh–Taylor hydrodynamic instabilities seeded by high-mode ($20 < \ell < 200$) ablator-surface mass perturbations from intrinsic CH surface roughness, the fill tube, or microscopic dust particles can mix ablator material into the interior of the DT-fuel layer if the initial amplitudes and growth during the acceleration phase are sufficiently large (i.e., hot-spot mix) [12]. Hydrodynamic simulations indicate ablator material that gets into the hot spot largely consists of material that originated at the ablation surface and ''bubbled'' through the ablator and DT-ice layers [12]. Another physical mechanism for hot-spot mix arises at the material interface between the ablator and DT-ice layer if the density of the ablator is less than the density of the DT-ice. This would cause the ablator–DT-ice interface to be unstable to the classical Rayleigh-Taylor hydrodynamic instability during the acceleration phase, resulting in bubbles of material from the innermost part of the ablator mixing through the DT-ice layer. Identifying the major physical mechanism

responsible for hot-spot mix would focus future mitigation efforts in inertial confinement fusion research.

This Letter presents the first evidence that the ablation-front instability is primarily responsible for hot-spot mix in ignition-scale implosions and provides a quantitative estimate of the amount of ablator mass mixed into the hot spot. Different tracer materials are placed at known radial positions in the plastic ablator [12] and their initial locations and concentrations are measured [15]. The mixing of plastic ablator material, doped with Cu or Ge dopants, deep into the hot spot is diagnosed with x-ray spectroscopy [16] on the NIF. The Cu and Ge dopants will only be ionized to the K shell and emit K-shell emission if they are mixed from the ablator into the hot spot. Since the Cu and Ge dopants are placed at different radial locations in the plastic ablator (i.e., the Ge-doped CH layer surrounds the Cu-doped CH layer), their spectroscopic signature indicates which layer is mixing into the hot spot. The ablation front burns well into the Ge-doped layer, but does not reach the Cu-doped layer. The majority of the observed hot-spot mix mass contains mass from the ablation-surface region (i.e., the Ge-doped CH), consistent with the hypothesis that the ablation-front instability is primarily responsible for the hot-spot mix. These experimental observations are important for ICF because enhanced radiative losses of the hot spot by the mix mass could be the reason for the current targets on the NIF not igniting. The strategy to control hot-spot mix from the ablation-front instability involves reducing the capsule surface-mass perturbations, reducing the growth factors of the hydrodynamic instability [12], or changing to another ablator material (e.g., Cu-doped Be [17]).

A schematic of the ignition-scale target used to diagnose the ablator mix mass in the hot spot with x-ray spectroscopy is shown in Fig. 1 [12]. It has an outside radius of 1130 μm, a 195-μm-thick tri-doped CH ablator, and a 69-μm-thick DT-ice layer. The initial masses of the DT vapor, the DT shell, and the ablator are 820 ng, 1.4×10^5 ng, and 2.6×10^6 ng, respectively. Ablation of the inner wall of the DT-fuel layer increases the DT mass in the hot spot. The unablated mass of the tri-doped CH ablator is 10% of the initial shell mass. The outermost layer (i.e., layer 5) is pure CH and is 138 μm thick. The Si dopant in layers 2, 3, and 4 is the usual preheat shield [18], and trace amounts (i.e., $\sim$0.1% atomic) of Cu (layer 1) and Ge (layers 2 and 3) are added at different radial locations to study the origin of the hot-spot mix mass. The x-ray ablation front burns through layers 5 and 4 and well into the Ge-doped CH layer 3, but it does not reach the Cu-doped CH layer. Therefore, if the hot-spot mix mass is due to ablator material originating at the ablation front that "bubbles" through the ablator and DT ice [12], the mix mass will consist of Ge-doped CH, not Cu-doped CH. The amount of hot-spot mix is determined from the absolute brightness of the emergent Cu and Ge K-shell emission using a detailed atomic physics

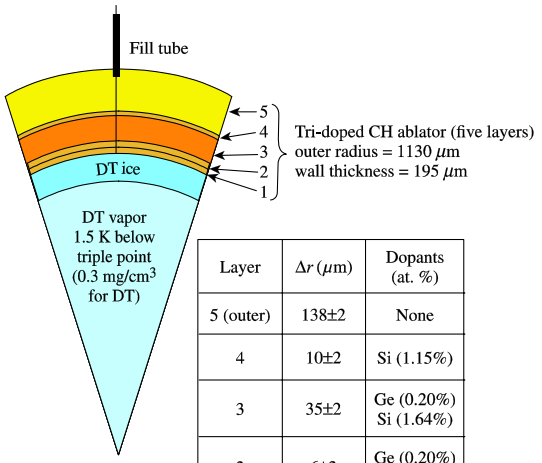

Layer	Δr (μm)	Dopants (at. %)
5 (outer)	138±2	None
4	10±2	Si (1.15%)
3	35±2	Ge (0.20%) Si (1.64%)
2	6±2	Ge (0.20%) Si (0.87%)
1	6±2	Cu (0.14%)
DT ice	69	None
DT vapor (inner)	935	None

FIG. 1 (color online). Schematic of an ignition target with a tri-doped CH ablator and a cryogenic DT layer. The Si dopant is a preheat shield. The Cu and Ge dopants are placed at different radial locations to determine the origin of the hot-spot mix mass. The DT fuel is transported to the interior of the plastic ablator using a fill tube.

model [19]. Two other types of CH ablators were studied. One, a "co-doped" ablator has no Cu dopant and its layers are composed as follows: layer 1 has only a Ge dopant (0.1% atomic); layer 2 has a Ge dopant (0.1% atomic) and a Si dopant (1.93% atomic); and layer 3 has a Ge dopant (0.1% atomic) and a Si dopant (3.40%). The second type of ablator is called the Rev. 5 ablator [10], which has only a Ge dopant; layers 1 and 5 are pure CH and a Ge dopant with 0.5%, 1.0%, and 0.5% (atomic) is in layers 2, 3, and 4, respectively. DT and hydrodynamically equivalent tritium-hydrogen-deuterium (THD) cryogenic targets [20] were examined.

The time-integrated, 1D imaging hot-spot x-ray spectrometer (HSXRS) provided spectral coverage in the 6 to 16 keV range for analysis of the Cu and Ge K-shell emission [21]. The HSXRS combines a slit aperture with a 100-μm width and a pentaerythritol (PET) Bragg crystal to record 1D spectral images of the implosion core with a magnification of about 11, a spatial resolution of approximately 100 μm in the target plane, and a spectral resolving power of 300–800 [21]. The accuracy of the HSXRS photometric calibration is $\pm$50%. Figure 2 shows a spatially integrated x-ray spectrum of the hot spot measured on an ignition target with a tri-doped CH ablator of HSXRS (black curve), highlighting the spectral features attributed to cold Cu and Ge in the compressed ablator (Cu and Ge Kα fluorescent emission and the Cu and Ge K-edge absorption) and, most importantly, the emission from the

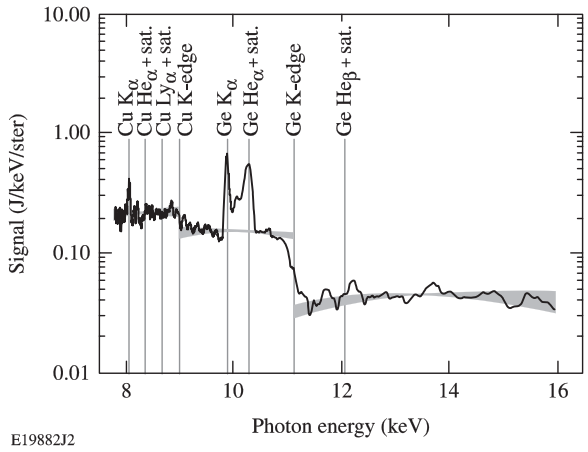

FIG. 2. Measured x-ray spectrum for an ignition target with a tri-doped ablator (black curve). The x-ray continuum from the hot spot transmitted through the compressed shell is modeled (gray curve) assuming the x-ray continuum and the shell optical thickness scale with photon energy ($h\nu$) as $e^{-h\nu/\mathrm{kT}}$ and $h\nu^{-3}$, respectively.

highly ionized Ge in the hot-spot mix mass between 10 and 10.5 keV. He-like Ge is the highest charge state observed. Any emission from highly ionized Cu in the hot spot is below the detection threshold of the spectrometer, as observed by examining the spectral range between 8 and 9 keV in Fig. 2. The gray curve in Fig. 2 is a derived hot-spot continuum spectrum, assuming the hot-spot x-ray continuum scales as $e^{-h\nu/kT}$ and the shell optical thickness scales as $h\nu^{-3}$, where $h\nu$ is the photon energy.

The 9.7- to 10.8-keV photon-energy range, containing emission from the hot spot and the compressed shell, is highlighted in Fig. 3 for the ignition target with the tri-doped CH ablator. In this plot the hot-spot x-ray continuum was subtracted and a correction for compressed ablator x-ray absorption was applied. This photon-energy range contains a rich spectrum of line emission from Ge He-like resonance $1s^2 - 1s2p(1\mathrm{P})$ and intercombination $1s^2 - 1s2p(3\mathrm{P})$ transitions, as well as from their $1s^2(2s, 2p)^l - 1s2p(2s, 2p)^l$ satellite transitions with $l = 1, 2, 3$, corresponding to the Li-, Be-, B-like Ge charge states. This spectral envelope, called the Ge He_α + satellite emission, is from the hot spot and is sensitive to variations in the electron temperature (T_e), electron density (n_e), and Ge areal density of the mix mass [22]. Around the time of peak compression a cold, dense shell surrounds a central hot spot. Most of the Ge remains in the compressed shell and absorbs x rays from the hot spot. Depending on the temperature of the shell, this absorption manifests as either Ge Kα emission or Ge $1s - 2p$ absorption features [22]. The feature between the Ge Kα and the Ge He_α + satellite emission in Fig. 3 is primarily photo-excited inner shell transitions from low charge states of Ge (i.e., Ne-, O-, F-, N-, or C-like). They exist on the edge of the hot spot with $T_e \sim 0.5$ keV and $n_e = 2 \times 10^{25}$ cm^{-3}. This signal may

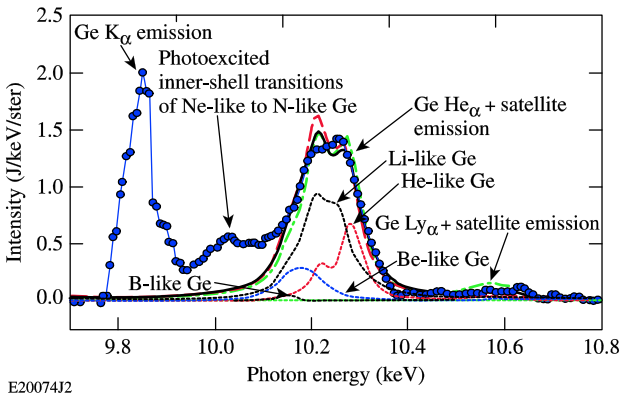

FIG. 3 (color online). Measured x-ray spectrum in the 9.7 to 10.8 keV range (blue circle) for an ignition target with tri-doped CH ablator. The Ge He_α + satellite emission is from the hot-spot mix mass. The Ge Kα emission is from the compressed shell. The feature around 10 keV is primarily photoexcited inner shell transitions from low charge states of Ge (i.e., Ne-, O-, F-, N-, or C-like) existing on the edge of the hot spot. The amount of Ge-doped CH ablator mixed into the hot spot is inferred from the modeled Ge He_α + satellite spectrum (best fit = solid black curve, 1σ spectral fits = dashed red and dashed-dotted green curves). The dotted lines show the spectral components of the best fit from B-, Be-, Li-, and He-like charge states of Ge.

indicate a significant amount of ablator mass that has mixed through the DT-ice layer to the edge of the hot spot, but not deep into the hot spot. Only the Ge He_α + satellite emission is used to diagnose the mix mass in the hot spot.

The mix mass is crudely modeled as CH-ablator mass doped with the same atomic fraction of Ge (Cu) in the CH ablator, at the same single n_e and T_e, and with areal densities of Ge-doped CH (ρR_{CHGe}) and Ge (ρR_{Ge}) that characterizes the mix-mass structure by an effective scale length or, more precisely, an average photon escape path. The mix-mass length is micron scale, consistent with a number of mix-mass objects (e.g., spheres) that varies from a few up to thousands, depending on the implosion. Although this approximation is applied to make the analysis tractable, spatial gradients in the plasma conditions of the mix mass material are likely. A detailed atomic and radiation physics model [19] is used to estimate the amount of mix mass from the Ge K-shell line spectrum as follows: The temperature- and density-dependent emissivity model gives the total emission per Ge mass within the Ge He_α + satellite feature. The spectral fit includes self-absorption–coupled level kinetics, giving an estimate of ρR_{Ge} in each mix-mass sphere. In the atomic model, the Ne- through H-like species are represented with detailed-configuration accounting (DCA), including all single excitations through $n = 10$ and all double excitations through $n = 3$; important line-emitting configurations are split. The Stark broadening of the Ge line shapes was calculated using the MERL code [23], but is not significant for $n_e < 10^{25}$ cm^{-3}.

The calculated emergent intensity distribution is sensitive to variations in n_e, T_e, and ρR_{Ge}. The measured spectra are compared with modeled spectra, including instrumental broadening effects, for several thousand combinations of n_e, T_e, and ρR_{Ge}, and the best match is determined based on a least squares fit. The amount of Ge mix mass is then determined from the inferred plasma conditions and by comparing the brightness per mass to the total measured brightness of the Ge He_α + satellite measurement.

The hot-spot mix-mass analysis assumes uniform plasma conditions lasting 125 ps (x-ray burn width of the implosion [24]) for the DT and THD implosions, the mix mass has the same dopant level as the shell, and 30% shell transmission for the Ge He_α + satellite feature (per 1D hydrodynamic simulations). This estimate of shell transmission represents a lower limit for the experiment leading to a conservative estimate of hot-spot mix mass. The modeled spectra are shown in Fig. 3, with the black curve representing the best fit (i.e., minimum χ^2) and the dashed red and dashed-dotted green curves representing 1σ spectral fits. The latter define the upper and lower limits of hot-spot mix mass. The dotted lines in Fig. 3 show the spectral components of the best fit from the Ge charge states. The inferred quantities for the DT implosion are $n_e = 0.9(+0.1, -0.5) \times 10^{25}$ cm^{-3}, $T_e = 3.0(+0.6, -0.4)$ keV, $\rho R_{\mathrm{Ge}} = 0.325(-0.1, -0.025)$ mg/cm^2, and a total mix mass of $34(-13, +50)$ ng. The total mix mass is composed of C, H, and Ge assuming the initial stoichiometry of the Ge-doped ablator layer.

Since the Cu He_α + satellite emission signal was below detection threshold of the spectrometer, an upper bound of mix mass from the Cu-doped layer of 2 ± 1 ng was estimated for the noise level of the spectrometer. The plasma conditions of the Cu-doped mix mass were assumed to be the same as the Ge-doped mix mass (inferred from the x-ray spectroscopy), and a 20% shell transmission was assumed for the Cu He_α + satellite emission (per 1D hydrodynamic simulations). The hot-spot mix mass from the Cu-doped layer is a factor of 17 lower than the mix mass from the Ge-doped layer. These observations indicate the ablation-front instability is primarily responsible for the hot spot mix, not the classical Rayleigh-Taylor hydrodynamic instability at the ablator–DT-ice interface during the acceleration phase.

The measured neutron yield of the ignition-scale implosions normalized to the 2D simulation prediction without alpha heating is plotted for seven implosions as a function of the hot-spot mix mass inferred from the x-ray spectroscopy in Fig. 4. The dashed vertical line indicates the NIF requirement that low radiative cooling requires that the CH(Ge) hot-spot mix mass be less than 75 ng [10]. Low neutron yields and hot-spot mix mass between $34(-13, +50)$ ng and $4000(-2970, +17\,160)$ ng are observed. There is a sharp drop in neutron yield around the 75-ng limit and the lowest yield has the highest mix mass. The experimentally inferred values of hot-spot mix mass may represent a lower bound since the x-ray spectroscopy is only sensitive to the portions of the ablator that are doped with the Cu or Ge. As shown in Fig. 1, the outermost portion of the ablator (layer 5) is pure CH. According to the hydrodynamic simulations, the shell reaches one half of the peak velocity around the time this layer is completely ablated. Any hot-spot mix mass from the pure CH ablator cannot be detected with x-ray spectroscopy. The amount of mix mass inferred from the diagnostic technique of enhanced x-ray production relative to neutron yield [14] is systematically a few times higher than the value inferred from the x-ray spectroscopy technique. The higher inferred value could be due to the hot-spot mix occurring during the ablation of the pure CH ablator layer.

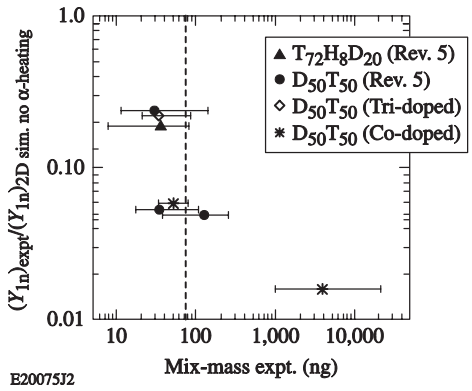

FIG. 4. The measured neutron yield normalized to the 2D simulated neutron yield with alpha heating turned off is compared to the spectroscopically diagnosed hot-spot mix mass. The dashed vertical line indicates the NIF requirement for the CH(Ge) hot-spot mix mass to be less than 75 ng.

The authors acknowledge the excellent operation of the National Ignition Facility and helpful suggestions from M. Key. This work was supported by the U.S. Department of Energy Office of Inertial Confinement Fusion under Cooperative Agreement No. DE-FC52-08NA28302.

*Also at Departments of Mechanical Engineering and Physics and Astronomy, University of Rochester, Rochester, NY 14623, USA.

[1] J. D. Lindl, P. Amendt, R. L. Berger, S. G. Glendinning, S. H. Glenzer, S. W. Haan, R. L. Kauffman, O. L. Landen, and L. J. Suter, Phys. Plasmas **11**, 339 (2004).
[2] S. H. Glenzer *et al.*, Science **327**, 1228 (2010).
[3] G. H. Miller, E. I. Moses, and C. R. Wuest, Opt. Eng. **43**, 2841 (2004).
[4] T. R. Boehly *et al.*, Phys. Plasmas **16**, 056302 (2009).
[5] O. L. Landen *et al.*, Phys. Plasmas **18**, 051002 (2011).
[6] D. G. Hicks *et al.*, Phys. Plasmas **19**, 122702 (2012).
[7] P. Michel *et al.*, Phys. Plasmas **17**, 056305 (2010).
[8] G. A. Kyrala *et al.*, Phys. Plasmas **18**, 056307 (2011).
[9] M. J. Edwards *et al.*, Phys. Plasmas **18**, 051003 (2011).

[10] S. W. Haan *et al.*, Phys. Plasmas **18**, 051001 (2011).
[11] A. J. Martin, R. J. Simms, and R. B. Jacobs, J. Vac. Sci. Technol. A **6**, 1885 (1988); B. J. Kozioziemski *et al.*, Fusion Sci. Technol. **59**, 14 (2011).
[12] B. A. Hammel, S. W. Haan, D. S. Clark, M. J. Edwards, S. H. Langer, M. M. Marinak, M. V. Patel, J. D. Salmonson, and H. A. Scott, High Energy Density Phys. **6**, 171 (2010); B. A. Hammel *et al.*, Phys. Plasmas **18**, 056310 (2011).
[13] G. A. Kyrala *et al.*, Rev. Sci. Instrum. **81**, 10E316 (2010).
[14] T. Ma, N. Izumi, R. Tommasini, D. K. Bradley, C. J. Cerjan, T. Döppner, M. J. Edwards, S. W. Haan, M. H. Key, J. L. Kline, A. J. MacKinnon, H. S. Park, P. K. Patel, B. A. Remington, V. A. Smalyuk, P. T. Springer, R. P. J. Town, S. V. Weber, and S. H. Glenzer, Bull. Am. Phys. Soc. **57**, 245 (2012); T. Ma *et al.* (to be published).
[15] H. Huang, R. B. Stephens, A. Nikroo, S. A. Eddinger, K. C. Chen, H. W. Xu, K. A. Moreno, K. P. Youngblood, and M. Skelton, Fusion Sci. Technol. **51**, 530 (2007); H. Huang, A. Nikroo, R. B. Stephens, S. A. Eddinger, D. R. Wall, K. A. Moreno, and H. W. Xu, Fusion Sci. Technol. **55**, 356 (2009).
[16] H. R. Griem, *Principles of Plasma Spectroscopy* (Cambridge University Press, Cambridge, England, 1997).
[17] P. A. Bradley and D. C. Wilson, Bull. Am. Phys. Soc. **41**, 1557 (1996); Phys. Plasmas **8**, 3724 (2001).
[18] D. S. Clark, S. W. Haan, B. A. Hammel, J. D. Salmonson, D. A. Callahan, and R. P. J. Town, Phys. Plasmas **17**, 052703 (2010).
[19] J. J. MacFarlane, I. E. Golovkin, P. Wang, P. R. Woodruff, and N. A. Pereyra, High Energy Density Phys. **3**, 181 (2007).
[20] A. J. MacKinnon *et al.*, Phys. Rev. Lett. **108**, 215005 (2012).
[21] S. P. Regan *et al.* (to be published).
[22] S. P. Regan *et al.*, *The 17th International Conference on Atomic Processes in Plasmas (ICAPiP) AIP Conference Proceedings 1438*, edited by K. Aggarwal and F. Shearer (American Institute of Physics, New York, 2012), p. 49.
[23] R. C. Mancini, D. P. Kilcrease, L. A. Woltz, and C. F. Hooper, Comput. Phys. Commun. **63**, 314 (1991).
[24] D. H. Edgell, D. K. Bradley, E. J. Bond, S. Burns, D. A. Callahan, J. Celeste, M. J. Eckart, V. Yu. Glebov, D. S. Hey, G. Lacaille, J. D. Kilkenny, J. Kimbrough, A. J. Mackinnon, J. Magoon, J. Parker, T. C. Sangster, M. J. Shoup III, C. Stoeckl, T. Thomas, and A. MacPhee, Rev. Sci. Instrum. **83**, 10E119 (2012).